A GSM/EDGE/WCDMA adaptive series-LC matching network using RF-MEMS switches

A GSM/EDGE/WCDMA Adaptive Series-LC Matching Network Using RF-MEMS Switches

André van Bezooijen, *Member, IEEE*, Maurice A. de Jongh, Christophe Chanlo, Lennart C. H. Ruijs, Freek van Straten, *Member, IEEE*, Reza Mahmoudi, *Member, IEEE*, and Arthur H. M. van Roermund, *Senior Member, IEEE*

***Abstract*—To preserve link quality of mobile phones, under fluctuating user conditions, an adaptively controlled series-LC matching circuit is presented for multi-band and multi-mode operation. Following a bottom-up approach, we discuss the design of an RF-MEMS unit cell for the construction of a 5-bit switched capacitor array. To reduce dielectric charging of the RF-MEMS devices their average biasing voltage is minimized by applying a bipolar waveform with a small high/low duty-cycle obtained from a high-voltage driver IC. RF-MEMS capacitive switches are applied because of their high linearity, low loss, large tuning range, and easy control in the discrete domain. Application specific RF-MEMS pull-in and pull-out voltage requirements are derived. An impedance phase detector is used to feed mismatch information to an up-down counter providing robust iterative control. The measured MEMS array capacitance tuning ratio is almost a factor 10. Module insertion loss is 0.5 dB at low-band and high-band. Harmonic distortion is less than −85 dBc at 35 dBm output power and the EVM, measured in EDGE-mode, is less than 1% at 27 dBm. The adaptively controlled module, connected to a planar inverted-F antenna, shows desired impedance correction. For extreme hand-effects the maximum module impedance correction at 900 MHz is $-75j\Omega$.**

***Index Terms*—Adaptive filters, impedance matching, micro-electromechanical devices, phase detection, power amplifiers, switched capacitor filters.**

I. Introduction

LINK quality of cellular phones suffers from antenna mismatch that is caused by the narrow bandwidth of miniaturized high-Q antennas and by detuning of the antenna resonance frequency [1], [2] due to fluctuating body-effects and changes in phone form-factor. Mismatch of the antenna impedance results in reduced maximum field strength and deteriorates modulation quality [3], receiver sensitivity and power amplifier efficiency. Two solutions to these problems are well known.

As a first solution, isolators are used, especially in single-band CDMA One phones, to preserve linearity under mismatch conditions. However, they do not preserve maximum field strength and power efficiency because isolators absorb (the reflected) power. Moreover, for multi-band phones the use of isolators is not attractive because, due to their narrow bandwidth, multiple isolators are required that are bulky and cannot easily be integrated with other front-end functions.

As a secondary solution, adaptive antenna matching techniques [4]–[7] can be applied to maintain link quality. This method is more attractive because it preserves maximum field strength, power amplifier linearity, receiver sensitivity, and power efficiency of a phone simultaneously. In addition, for multi-band phones only one adaptive matching network is required, because tunable LC-networks can be designed to cover wide bandwidths. Furthermore, adaptive antenna matching enables the use of even further miniaturized (higher Q) antennas because it compensates for mismatch caused by limited bandwidth.

Unfortunately, the use of adaptive matching networks, in cellular phones, is hampered by very demanding requirements on linearity, insertion loss, and tuning range. Research on barium-strontium-titanate (BST) [8] and silicon varactors [9] have resulted in continuously tunable, linear, and low loss devices. However, their effective tuning range, limited by forward biasing and breakdown under large signal conditions, is only a factor of 3. A larger effective tuning range and high linearity is obtained by CMOS switches on sapphire [10], [11] and SOI [12], but their $R_{\mathrm{ON}} \cdot C_{\mathrm{OFF}}$ product is still large compared to that of capacitive MEMS (micro-electromechanical system) switches. CMOS switches are controlled by low voltages (3 V) and, in principle, the technology can be used to implement mismatch detectors and control logic, which might result in a high level of integration. RF-MEMS capacitive switches are well known for their exceptionally large tuning range, high linearity, and very low loss [13], [14], but they still suffer from dielectric charging.

In this paper, an adaptively controlled matching network is presented [15] that compensates the imaginary part of the antenna impedance. We will exploit the capabilities of capacitive RF-MEMS switches among which its large tuning range. As a bottom-up approach, we discuss the design of an RF-MEMS unit cell that is used for the realization of a variable capacitor implemented as a 5-bit binary weighted array. It is fabricated in an RF-MEMS technology [16], [17] that is optimized for multi-standard mobile phone applications. Communication protocol specific requirements on minimum RF-MEMS pull-in and pull-out voltage are derived, which dictates the actuation voltages needed. These actuation voltages are generated by a high-voltage driver IC providing a bipolar biasing wave-form

Manuscript received December 17, 2007; revised June 9, 2008. Current version published October 8, 2008.

A. van Bezooijen, M. A. de Jongh, C. Chanlo, and L. C. H. Ruijs were with NXP Semiconductors, 6534 AE Nijmegen, The Netherlands. They are now with EPCOS Netherlands B.V., Bijsterhuizen 11-22, 6546 AS, Nijmegen, The Netherlands (e-mail: andre.van.bezooijen@epcos.com; maurice.de.jongh@epcos.com; christophe.chanlo@epcos.com; lennart.ruijs@epcos.com).

F. van Straten is with NXP Semiconductors, 6534 AE Nijmegen, The Netherlands (e-mail: freek.van.straten@nxp.com).

R. Mahmoudi and A. H. M. van Roermund are with the Eindhoven University of Technology, 5600 MB Eindhoven, The Netherlands (e-mail: m.mahmoudi@tue.nl; a.h.m.v.Roermund@tue.nl).

Digital Object Identifier 10.1109/JSSC.2008.2004334

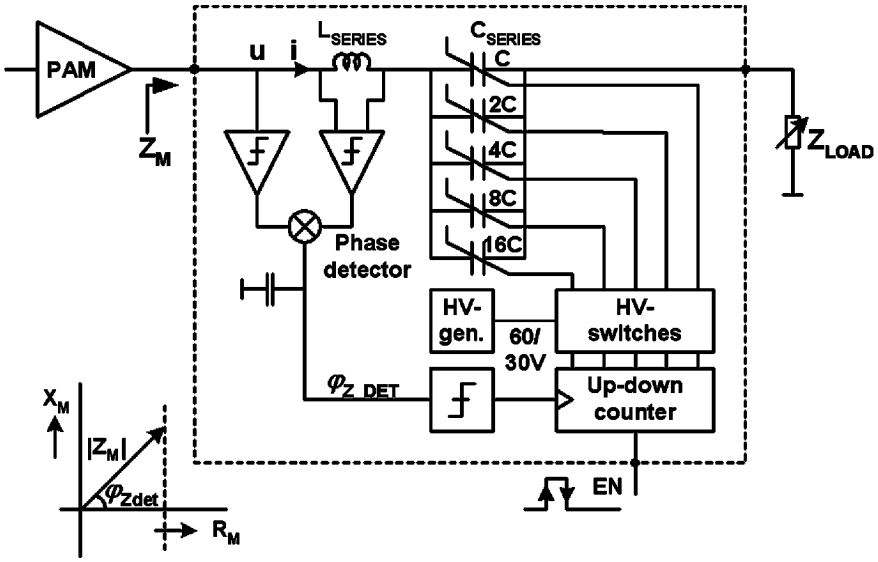

Fig. 1. Block diagram of an adaptive series-LC matching network. It compensates the reactive part of the load impedance by controlling the detected phase $\phi_{\mathrm{Z\_DET}}$ of the matched impedance to zero.

with a low 60/30 V actuation/hold duty-cycle in order to minimize dielectric charging and thus to improve MEMS reliability. A wafer-to-wafer bonding method is applied to obtain a sufficiently hermetic package [18].

II. Adaptive Tuning System

In mobile phones, often a planar inverted-F antenna (PIFA) is used that behaves as a series resonance circuit at both low-band $(\mathrm{LB} \sim 900\ \mathrm{MHz})$ and high-band $(\mathrm{HB} \sim 1800\ \mathrm{MHz})$. Body-effects cause mainly a down shift in resonance frequency resulting in an more inductive impedance at the antenna feed point. We have chosen for correction by a tunable series-LC matching network because it is the simplest network that effectively compensates the inductive antenna behavior when it is placed close to the antenna feed point. A block diagram of the adaptively controlled series-LC matching network is depicted in Fig. 1. It comprises a tunable 5-bit switched capacitor array, high-voltage MEMS biasing switches, a high-voltage generator, a phase detector, and an up/down counter.

Mismatch information is given by the phase of the matched impedance Z_M at the network input. It is determined by the phase difference between the network input voltage u and its input current i. The voltage u is measured single-ended, whereas a measure of the branch current i is obtained from the differential voltage across the sensing inductor L_{SERIES}. The detected phase $\phi_{\mathrm{Z\_DET}}$ is obtained from a mixer that is driven by hard limited input signals and is given by [19], [20]

$$\varphi_{\mathrm{Z\_DET}} = \frac{2}{\pi}(\varphi_u - \varphi_i). \tag{1}$$

The phase detector output signal $\phi_{\mathrm{Z\_DET}}$ is fed to a limiter to determine the sign of the phase. Depending on this sign the counter will either increase or decrease its output value in steps of 1 LSB (least significant bit). The counter outputs control the high-voltage switches to bias the RF-MEMS devices of the switched capacitor array. Updates of the array are made under control of a baseband enable signal *EN* that can be synchronized to the frame repetition rate of the GSM/EDGE/WCDMA transmission protocols. Consequently, the loop controls the phase of the detected impedance $\phi_{\mathrm{Z\_DET}}$ to zero step by step, keeping phase transients of the transmitted signal small.

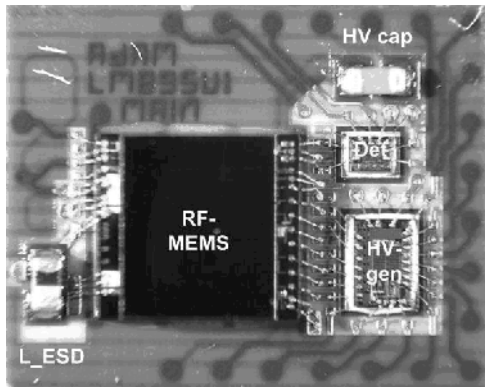

Fig. 2. Photograph of the adaptive antenna matching module showing the packaged RF-MEMS, high-voltage generator, and impedance phase detector dice.

In this concept, the series inductor L_{SERIES} has three functions. First, it provides impedance transformation as part of the matching network. Second, it acts as an sensing element from which information on mismatch is obtained. Third, it provides $+90$ degrees phase shift required for proper phase detection.

The photograph in Fig. 2 shows the adaptive antenna matching module that consists of a Si-capped RF-MEMS die, a detector die, and a high-voltage generator die, all wire bonded to laminate. The module contains two surface mounted device (SMD) components: a 1 nF high-voltage buffer capacitor and an inductor for ESD protection at the antenna terminal.

A. Series-LC Network

The matched impedance Z_M at the input of a series-LC network, as shown in Fig. 3, is defined as

$$Z_M = R_M + jX_M \tag{2}$$

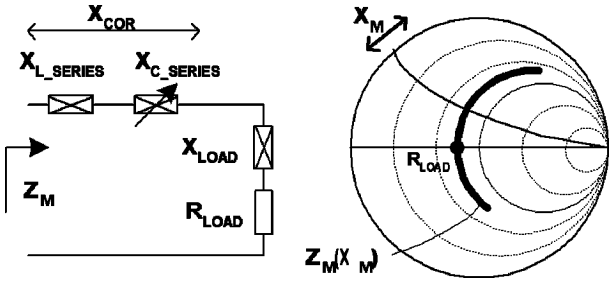

Fig. 3. Tunable series-LC network providing correction for inductive and capacitive load reactance visualized on a Smith chart.

in which the matched resistance R_M is given by

$$R_M = R_{\mathrm{LOAD}} \tag{3}$$

and the matched reactance X_M by

$$X_M = X_{L_{\mathrm{SERIES}}} + X_{C_{\mathrm{SERIES}}} + X_{\mathrm{LOAD}}. \tag{4}$$

Tuning the series capacitor value C_{SERIES} changes the matched reactance X_M over a circle segment of constant resistance R_{LOAD} as visualized in the Smith chart in bold. It is a monotone function of the tunable reactance X_{C_SERIES}. The matched resistance R_M is equal to the load resistance R_{LOAD} and fully independent of the tunable reactance X_{C_SERIES}. Hence, the proposed concept cannot compensate for fluctuations in the real part of the antenna impedance.

B. Capacitance Tuning Range

In this section, we derive the capacitance ratio required to transform an arbitrary load reactance X_{LOAD} to a desired matched reactance X_M. As a first condition, we assume that the network must be able to tune a load reactance X_{LOAD1} to a matched reactance X_{M1}, at a minimum frequency f_1. As a second condition, the same network must be capable in tuning a load reactance X_{LOAD2} to a matched reactance X_{M2}, at a maximum frequency f_2. Rewriting (4) gives the series capacitor C_{SERIES} as

$$C_{\mathrm{SERIES}} = \frac{1}{2\pi f}\left(\frac{1}{X_{\mathrm{LOAD}} - X_M + X_{L_{\mathrm{SERIES}}}}\right). \tag{5}$$

From (5), the required capacitance ratio of the tunable series capacitor CR_{C_SERIES} can now be expressed as

$$CR_{C_{\mathrm{SERIES}}} = \frac{f_2}{f_1}\left\{\frac{X_{\mathrm{LOAD2}} - X_{M2} + X_{L_{\mathrm{SERIES2}}}}{X_{\mathrm{LOAD1}} - X_{M1} + X_{L_{\mathrm{SERIES1}}}}\right\}. \tag{6}$$

This equation reveals two important network properties. First, the required ratio becomes excessive when the denominator approaches zero, which occurs when the desired correction in capacitive reactance $|X_{\mathrm{LOAD1}} - X_{M1}|$ equals the reactance of the series inductor $|X_{L\_\mathrm{SERIES1}}|$. Hence, this tunable network is not very capable in correcting capacitive mismatches (but well capable in correcting inductive mismatches). Second, the required capacitance ratio is proportional to the ratio between the required maximum and minimum frequency of operation, which is important for multi-band applications. We have chosen for this tunable series-LC network because its tuning range fits to the typical behavior of PIFAs [21] that become inductive under the influence of body effects (see measurement results in Section IV). In addition, we exploit the large tuning range of RF-MEMS capacitive switches to meet tuning range requirements.

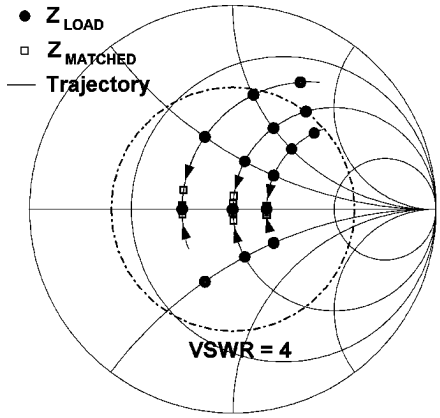

Fig. 4. Simulated impedance mismatch adaptation. The load impedances $30, 50, 70 + j(-25, 0, +25, +50, +75)\ \Omega$ are adapted to approximately $30, 50, 70\ \Omega$ over circle segments of constant resistance. $f = 900$ MHz.

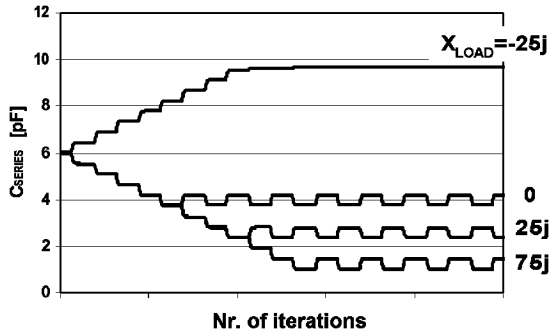

Fig. 5. Series capacitor value as a function of time (number of iterations) for the load impedances $50 + j(-25, 0, +25, +75)\ \Omega$. $f = 900$ MHz.

C. Simulations

The functionality of the adaptive series-LC matching network has been verified by ADS ENVELOPE[1] (a commercially available software package) simulations using behavioral models. Acquisition of the adaptive loop is simulated for the load impedances $(30, 50, 70) + j(-25, 0, +25, +50, +75)\ \Omega$, which are marked by solid dots in Fig. 4. The lines over circle segments of constant resistance show the trajectories of impedance adaptation as a function of time. Once the steady-state condition is reached, the matched impedances, designated by open squares, are clustered around three points close to the real axis of the Smith chart. Fig. 5 shows the corresponding series capacitor values, as a function of time (number of iterations), for the load impedances $50 + j(-25, 0, +25, +75)\ \Omega$. The capacitor value is initialized at 6 pF and adapts, in steps of 0.5 pF, to a minimum value of 1 pF for an inductive load of $+75j$ and to 10 pF for a capacitive load of $-25j$.

Obviously, a large inductive mismatch as well as a small capacitive mismatch (that correspond to expected PIFA feed point impedances) are well compensated by this series-LC network,

[1]Agilent Technologies, http://www.home.agilent.com

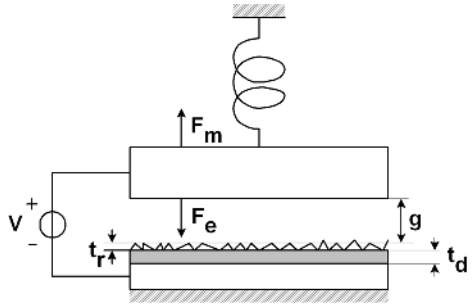

Fig. 6. RF-MEMS capacitive switch model including effective surface roughness.

TABLE I
REPRESENTATIVE RF-MEMS PROCESS AND DESIGN PARAMETER VALUES, CORRESPONDING UNIT CELL, AND ARRAY PROPERTIES

Process and design parameters		Unit cell properties (Section III-A)	
g_0	3 μm	C_{ON}	4.4 pF
t_r	0.1 μm	C_{OFF}	0.275 pF
t_d	0.5 μm	CR_{MEMS}	16
ε_r	5	U_{PI}	45 V
ε_0	8.85e-12 F/m	U_{PO}	6.6 V
A	200x500 μm	**Array properties (Section III-B)**	
k	200 N/m		
		r	3
		C_P	1 pF
		$C_{ARRAY\ MIN}$	2 pF
		$C_{ARRAY\ MAX}$	16 pF
		CR_{ARRAY}	8

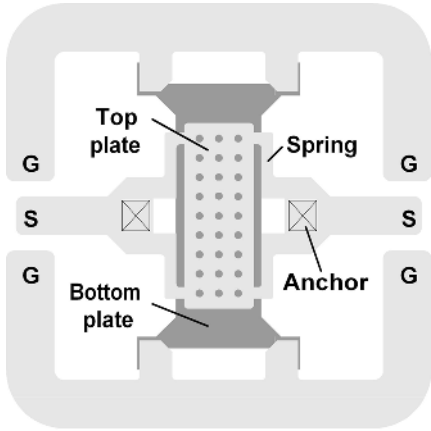

Fig. 7. Layout of a 4 pF RF-MEMS unit cell in an on-wafer ground-signal-ground RF characterization structure.

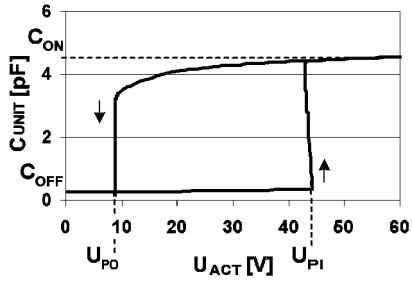

Fig. 8. Typical *CV* curve of an RF-MEMS capacitive switch as used as a unit cell in the 5-bit array.

requiring a capacitance tuning ratio of 10. Once, after approximately 10 iterations, acquisition of the loop is obtained a limit cycle oscillation of ± 1 LSB is visible that is caused by quantization of the capacitor value.

III. ADAPTIVE RF-MEMS SYSTEM DESIGN

As a bottom-up approach, we will now treat the design of an RF-MEMS unit cell, a 5-bit RF-MEMS array constructed out of such unit cells, and the high-voltage generator. In addition, application specific requirements on RF-MEMS pull-in and pull-out voltages are derived that determine the minimum voltage needed for actuation.

A. RF-MEMS Unit Cell

In theory [13], the capacitance of a MEMS device $C_{\rm MEMS}$ as function of the gap height g, depicted in Fig. 6, is given by

$$C_{\rm MEMS} = \frac{\varepsilon_0 A}{g + t_r + \frac{t_d}{\varepsilon_r}} \tag{7}$$

in which ε_0 is the free space dielectric constant, A is the effective MEMS capacitance area, t_r is the effective surface roughness of the beam and dielectric layer, modeled as an equivalent residual air gap, and t_d and ε_r are the thickness and relative dielectric constant of the dielectric layer. The MEMS capacitance ratio $CR_{\rm MEMS}$ between the ON and OFF capacitance of the MEMS device, given by the condition $g = 0$ and $g = g_0$ respectively, can now be written as

$$CR_{\rm MEMS} = 1 + \frac{g_0}{t_r + \frac{t_d}{\varepsilon_r}}. \tag{8}$$

Table I summarizes representative process and design parameter values and corresponding unit cell properties. Although roughness tends to halve the effective ON capacitance, an impressive tuning range of 16 is achieved for the intrinsic part of the device. In practice, however, bending of the top plate and parasitic capacitance of the springs will affect the ON and OFF capacitances, causing a reduction in tuning ratio. It is worthwhile noting that the adaptively controlled series-LC network is not sensitive to spreads in these parameters because it automatically compensates for deviations in capacitance value. Fig. 7 depicts a layout of the unit cell with a ground-signal-ground (GSG) connection for RF characterization. It consists of a rectangular top plate that is supported by four springs sharing two anchors as fixed points. A 3×9 pattern of holes at a pitch of 50 μm is used in the top plate for reduced squeeze film damping [22], which decreases the switching time to approximately 100 μs. A representative *CV* curve of the unit cell is shown in Fig. 8. The bistable device goes in ON-state when the actuation voltage $U_{\rm ACT}$ exceeds the pull-in voltage $U_{\rm PI}$ and switches back to the OFF-state when $U_{\rm ACT}$ becomes smaller than the pull-out voltage $U_{\rm PO}$.

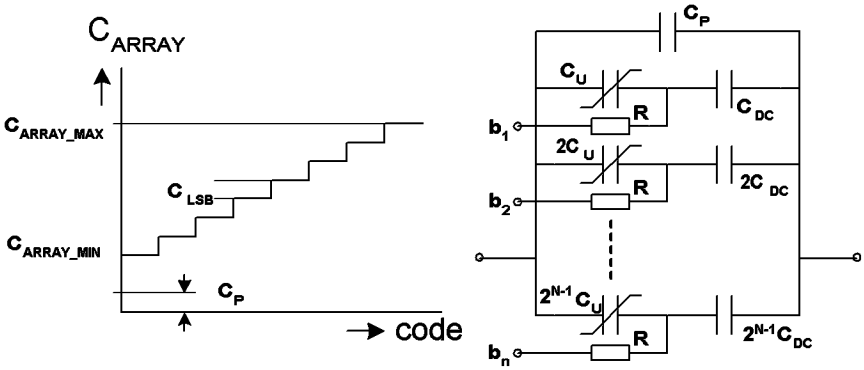

Fig. 9. Binary weighted RF-MEMS switched capacitor array, including DC-block capacitors and bias resistors, and its corresponding control curve.

B. RF-MEMS Switched Capacitor Array

The unit cell is used as building block for the realization of a 5-bit binary weighted switched capacitor array, conceptually depicted in Fig. 9. Each bit is activated via a bias control line b. In series with the RF-MEMS DC-blocking capacitors $C_{\rm DC}$ are required to isolate the biasing lines from each other for individual actuation. The resistors R provide RF isolation between the RF paths and the DC biasing lines and have high impedances to minimize insertion loss.

The minimum array capacitance $C_{\rm ARRAY\_MIN}$ is given by the sum of all RF-MEMS devices in the OFF-state plus a parasitic capacitance C_P in parallel to the array

$$C_{\rm ARRAY\_MIN} = \sum C_{\rm MEMS\_OFF\_n} + C_P. \tag{9}$$

Similarly, the maximum array capacitance $C_{\rm ARRAY\_MAX}$ is given by the sum of all RF-MEMS devices in the ON-state plus the same parasitic capacitance C_P

$$C_{\rm ARRAY\_MAX} = \frac{r}{r+1} \sum C_{\rm MEMS\_ON\_n} + C_P. \tag{10}$$

The factor $r/(r+1)$ stems from the DC-blocking capacitors that reduce the effective maximum capacitance of the array when the DC-blocking capacitance is made r times larger than the ON capacitance of the corresponding RF-MEMS device.

The capacitance ratio of the array $CR_{\rm ARRAY}$ can now be written as

$$CR_{\rm ARRAY} = \frac{\frac{r}{r+1} \sum C_{\rm MEMS\_ON\_n} + C_P}{\sum C_{\rm MEMS\_OFF\_n} + C_P}. \tag{11}$$

If the parasitic capacitance C_P can be neglected with respect to the sum of the ON capacitances, expressed by the numerator, the array capacitance ratio can be simplified to

$$CR_{\rm ARRAY} = \frac{r}{r+1} CR_{\rm MEMS} \frac{1}{1 + \frac{C_P}{\sum C_{\rm MEMS\_OFF\_n}}} \tag{12}$$

in which $CR_{\rm MEMS}$ is the MEMS ON/OFF capacitance ratio. Preferably, the parasitic capacitance is kept small with respect to the sum of the MEMS OFF capacitances.

Initially, the array was designed for a wide tuning range from approximately 1 pF to 15 pF with small steps of 0.5 pF to minimize the impedance step size. To achieve a reasonable compromise between control curve accuracy, required chip area, and capacitance ratio of the array, two major design choices have been made. First, the programmable capacitors are constructed out of parallel and series combinations of unit cells to secures monotony in the capacitor control curve and good matching of the pull-in and pull-out voltage over the wide range of capacitor values. Second, the unit cells are DC isolated from each other by MIM capacitors that are all similarly scaled by a capacitance ratio r of 3. Throughout the design process, a parasitic capacitance C_P of almost 1 pF turned out to be present, which tends to halve the array tuning range.

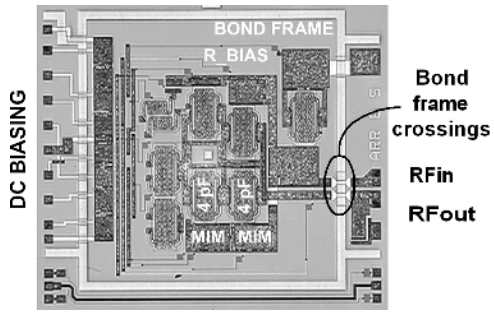

Fig. 10. Die photograph of a 5-bit switched capacitor array using 4 pF RF-MEMS unit cells with integrated DC-block MIM capacitors and bias resistors.

The array is implemented in an 5 k$\Omega \cdot$ cm high-resistive passive silicon technology [15]. Wafer-to-wafer bonding is applied to provide hermetic enclosure of the MEMS devices [18]. A die photograph of the array is depicted in Fig. 10.

C. Pull-In and Pull-Out Voltage Requirements

In this section, we derive minimum requirements for pull-in and pull-out voltage of the RF-MEMS unit cell. The pull-in voltage must be chosen sufficiently large in order to avoid self-actuation of the RF-MEMS due to RF. The pull-out voltage must be sufficiently large to avoid non-release of the RF-MEMS under hot-switching conditions. Self-actuation and non-release occur when the root mean square (RMS) voltage across the capacitor exceeds the pull-in voltage or pull-out voltage, respectively. Potentially, it prohibits adaptive impedance correction at high output power while a strong inductive mismatch is present, thus when adaptation is needed most. The RMS voltage across the variable series capacitor $U_{C\_\rm SERIES}$ is given by

$$U_{C\_\rm SERIES} = X_{C\_\rm SERIES} \cdot \sqrt{\frac{P_{\rm LOAD}}{R_{\rm LOAD}}} \tag{13}$$

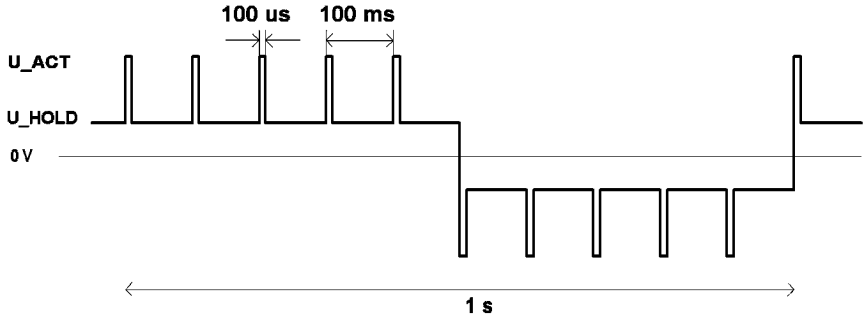

Fig. 11. Typical high-voltage generator output voltage waveform that provides reduced dielectric charging of RF-MEMS capacitive switches.

in which $P_{\rm LOAD}$ is the power delivered to the load resistance $R_{\rm LOAD}$ and $X_{C\_{\rm SERIES}}$ is the reactance of the variable series capacitor. Two operating conditions have been identified that dictate the required pull-in and pull-out voltage

First, the largest RMS voltage can be expected for low-band operation in GSM mode, while all RF-MEMS devices are in the OFF-state, because for this condition the maximum specified power $P_{\rm LOAD}$ and the reactance $X_{C\_{\rm SERIES}}$ are largest. For $P_{\rm LOAD} = 3.2$ W, $R_{\rm LOAD} = 50\ \Omega$, $C_{\rm SERIES} = 1$ pF, and $f =$ 900 MHz, $U_{C\_{\rm SERIES}}$ equals 45 V, according to (13). Hence, to avoid self-actuation the pull-in voltage must be at least 45 V.

Second, non-release of the beam occurs most likely for low-band operation in WCDMA mode, while only the LSB is in the ON-state, because in WCDMA mode hot-releasing of the RF-MEMS devices is needed (the protocol does not provide idle slots in which cold-switching could be done) and the reactance to be released is largest. For $P_{\rm LOAD} = 0.63$ W (maximum peak power), $R_{\rm LOAD} = 50\ \Omega$, $C_{\rm SERIES} = 1.5$ pF, and $f = 900$ MHz, $U_{C\_{\rm SERIES}}$ equals 13.2 V. To avoid non-release, the pull-out voltage must be at least 13.2 V, according to (13). This latter requirement is only relevant for the least significant bit, because when other bits are ON the voltage across the array remains significantly lower. Hence, we can reduce this pull-out voltage requirement to $13.2/2 = 6.6$ V by implementing the LSB by two RF-MEMS unit cells in series.

Because of these application-specific requirements, a high-voltage driver IC [23] is needed to bias the RF-MEMS devices, which will be discussed in Section III-D.

D. High-Voltage Driver IC

In order to actuate RF-MEMS devices with a 45 V pull-in voltage, as derived in Section III-C, a biasing voltage in excess of the pull-in voltage is needed. A major disadvantage of such a high actuation voltage is an enhanced charging of the MEMS dielectric layer, which causes a down-shift of the RF-MEMS pull-in and pull-out voltage that might result in self-actuation and non-release.

To combat shifts in *CV* curves, we apply a biasing schema with a minimum average actuation voltage that is accomplished by two measures: 1) a 60/30 V actuation voltage with small duty-cycle, and 2) a bipolar waveform to alternate the polarity of charging. A simplified (single-ended) biasing waveform is depicted in Fig. 11. During a relatively short interval (typically 100 μs), determined by the switching time of the RF-MEMS devices, a 60 V actuation voltage $U_{\rm ACT}$ is applied. Then, the actuation voltage of all MEMS devices in the ON-state goes down to a hold voltage $U_{\rm HOLD}$ of 30 V. This hold period lasts for a relatively long time (typically 10 to 100 ms), because a slow rate of impedance adaptation can be chosen to follow the even slower fluctuations in hand-effects. The polarity of actuation is changed at a typical rate of 1 Hz because the major dielectric charging mechanisms found are even slower. Fig. 12 shows a block diagram of the driver IC. It consists of a charge pump, high-voltage output switches, and two output voltage control loops. The charge pump, switched at 20 MHz, gradually charges a 1 nF SMD buffer capacitor under control of the 60 V stabilization loop. The 30 V control loop provides down-ramping and voltage stabilization of an internal node, which minimizes power losses of the charge pump. The 60/30 V waveform supplies the high-voltage output switches that are in parallel to separately bias each bit of the MEMS array. This high-voltage generator is implemented in a 120 V SOI process offering good isolation.

E. Module Insertion Loss

Power dissipation in the matching network must be kept small because it diminishes the effective transmitter efficiency enhancement obtained by improved impedance matching. For any power-matched two-port, the insertion loss IL can be defined as a ratio between dissipated power $P_{\rm DISS}$ and power delivered to the load $P_{\rm LOAD}$, as

$$IL = 10 \cdot \log\left(1 + \frac{P_{\rm DISS}}{P_{\rm LOAD}}\right). \tag{14}$$

The ratio between dissipated power and load power equals the ratio $R_{\rm SERIES}/R_{\rm LOAD}$ for a series loss resistance and the ratio $R_{\rm LOAD}/R_{\rm PAR}$ for a parallel loss resistance. Hence, for a 50 Ω load impedance, and ignoring second-order small terms, the insertion loss of the lumped equivalent series-LC network, shown in Fig. 13, can be expressed as

$$IL = 10 \cdot \log\left(1 + \frac{R_{L_{\rm SERIES}}}{R_{\rm LOAD}} + 2\frac{R_{\rm CROSS}}{R_{\rm LOAD}} + \frac{R_{\rm MEMS}}{R_{\rm LOAD}} + \frac{R_{\rm DC}}{R_{\rm LOAD}} + \frac{R_{\rm LOAD}}{R_{\rm BIAS}} + \frac{R_{\rm LOAD}}{R_{\rm SUB}}\right) \tag{15}$$

in which $R_{L\_{\rm SERIES}}$, $R_{\rm CROSS}$, $R_{\rm MEMS}$, $R_{\rm DC}$, $R_{\rm BIAS}$, and $R_{\rm SUB}$ are the equivalent loss resistances of the series inductor,

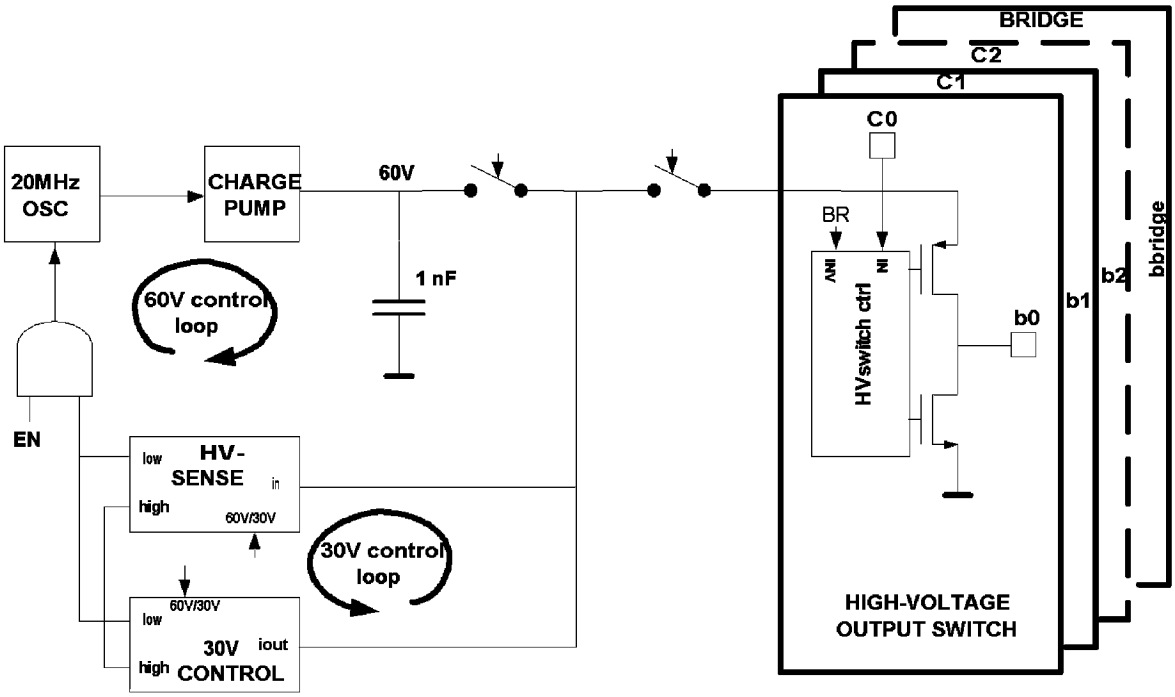

Fig. 12. Block diagram of the high-voltage generator providing a 60 V actuation and 30 V hold voltage. The bridge circuit allows for bipolar actuation of the RF-MEMS devices.

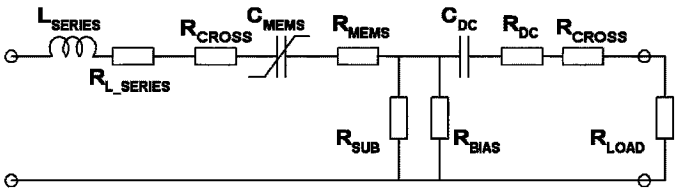

Fig. 13. Lumped equivalent circuit representing losses of the series-LC network.

bond frame crossing, RF-MEMS capacitors, DC-block capacitors, MEMS bias resistors, and the high-resistive silicon substrate, respectively. Estimates of these lumped equivalent loss resistances, given in Table II, have been obtained from simulations with SONNET[2] (a commercially available electromagnetic simulation package). Their values clearly illustrate that network losses are dominated by the loss resistance of the series inductor (implemented in laminate), the equivalent parallel MEMS biasing resistors, and the two bond frame crossings. These crossings introduce a significant amount of loss because their widths have been made small in order to minimize parasitic capacitance between the RF-path and the bond frame.

IV. Experimental Verification

In this section, we present, again as a bottom-up approach, experimental results on the MEMS switched capacitor array, followed by results on the entire module in open loop, and finally results on an adaptively controlling module connected to a planar inverted-F antenna (PIFA). For each specification, evaluation is done for the most demanding cellular phone mode of operation.

[2]Sonnet Software Inc., http://www.sonnetusa.com

TABLE II
Equivalent Loss Resistances and Their Contributions to the Insertion Loss of the Module

Equivalent loss resistance		IL
	[Ω]	[dB]
R_{L_SERIES}	1.3	0.11
$2{\cdot}R_{CROSS}$	0.6	0.05
R_{MEMS}	0.2	0.02
R_{DC}	0.2	0.02
R_{BIAS}	2k	0.11
R_{SUB}	5k	0.04
Total IL		0.35

A. RF-MEMS Switched Capacitor Array

The RF-MEMS array capacitance as a function of frequency is evaluated by on-wafer measurements and the results are compared to SONNET EM-simulation in Fig. 14(a). The capacitance in the OFF-state (00000) is approximately 2 pF for measurements and simulations, which is a factor 2 more than the initial design target. For the MSB ON-state (10000) the measured capacitance of 10 pF is only 20% larger than the simulated value of 8 pF, which might be caused by a difference in surface roughness. This results in a capacitance tuning range of almost 10.

Series resonance occurs due to a parasitic equivalent series inductance (ESL) of approximately 1.6 nH. Fortunately, for this module the ESL is harmless because it can easily be embedded in the desired series inductance.

For the various capacitance values, measurements and simulations show an insertion loss in the range of 0.3–0.5 dB at 1–2 GHz, as depicted in Fig. 14(b). At lower frequencies, the insertion loss increases drastically due to parasitic substrate shunt resistance, whereas at higher frequencies, series resistance and

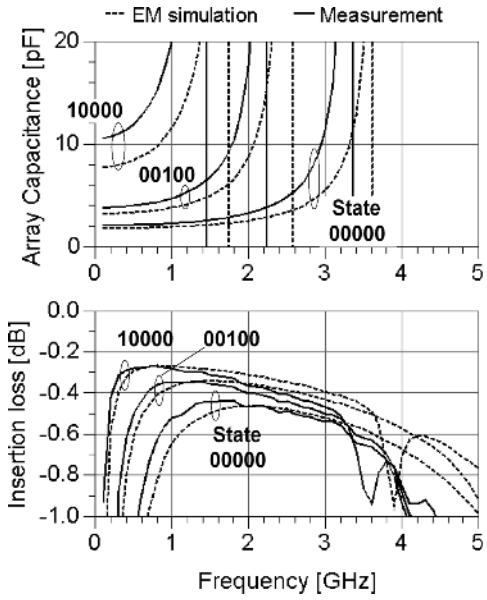

Fig. 14. (a) Simulated (dotted) and measured (solid) capacitance and (b) insertion loss of the 5-bit switched capacitor array for three different capacitor values.

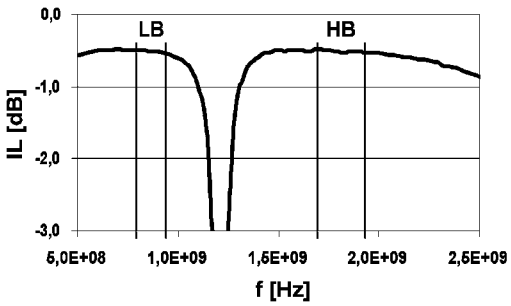

Fig. 15. Measured module insertion loss as function of frequency.

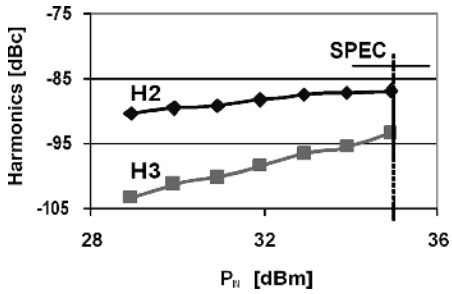

Fig. 16. Measured second- and third-order harmonic distortions as a function of input power.

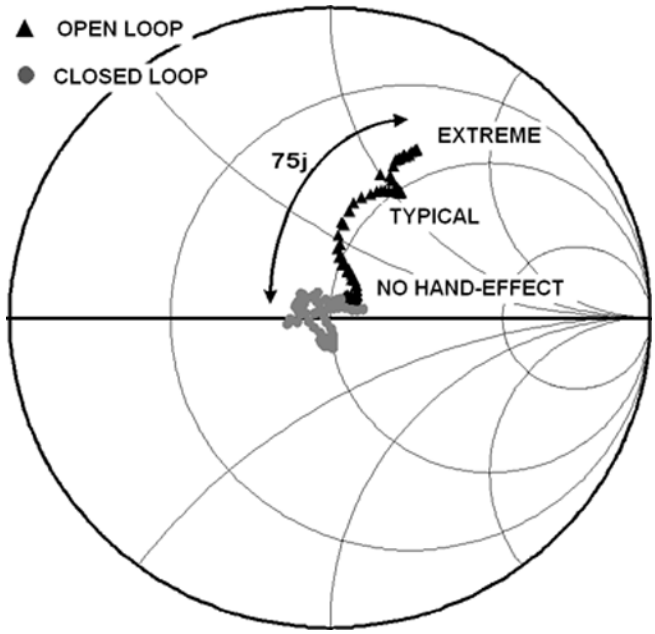

Fig. 17. Measured input impedance of the module when connected to a PIFA that is influenced by hand-effects, for open-loop and closed-loop conditions. $f = 900$ MHz.

skin effects of interconnect lines cause an increase in insertion loss.

B. Module Insertion Loss

Under 50 Ω and open-loop conditions, the insertion loss of the entire module is measured at approximately 0.5 dB for low-band and high-band, as shown in Fig. 15. These losses are predominantly caused by the series inductor and switched capacitor array biasing resistors, as discussed in Section III-E. The notch at 1.2 GHz results from a dual-banding network that has not been discussed in this paper.

C. Module Distortion

For a 50 Ω load and $f = 900$ MHz, the second- and third-order harmonic distortions of the module are measured as a function of power delivered to the load. These harmonic components, shown in Fig. 16, remain below −85 dBc up to 35 dBm output power, which is more than sufficient to meet the system specification of −83 dBc.

In a multi-standard environment, the reception of weak signals is hampered by strong interferers causing in-band inter-modulation products. Therefore, RF front-end inter-modulation distortion requirements are very demanding [24] and usually difficult to meet. We verified third-order inter-modulation distortion (IM3) for a +20 dBm wanted WCDMA signal at 1.96 MHz and a − 15 dBm interfering GSM signal at 1.76 MHz, causing an unwanted frequency component in the WCDMA receive band at 2.16 GHz. The IM3 component is measured at −117 dBm and is caused by the measurement set-up rather then by the module itself. It remains well below the specified −105 dBm. Hence, linearity specifications for operation in a multi-standard environment are well met.

Distortion due to modulation is verified in EDGE mode, because MEMS devices are most susceptible to amplitude modulation when a relatively large part of the power distribution falls within their mechanical bandwidth [25]. Up to 27 dBm output power, distortion due to EDGE modulation turns out to remain below the measurement set-up distortion level of approximately 1% for EVM and −70 dBc for ACPR. Both are well below typical RF front-end specifications of 2.5% and −60 dBc for EVM and ACPR, respectively.

D. Adaptive Module Connected to an Antenna

Measurements are performed on the complete module connected to a PIFA. First, the module input impedance is measured for an open-loop condition in which the MEMS array setting is fixed. A hand is moved towards the PIFA, touching its enclosure, and then covering it completely. During this action, the impedance moves away from the center of the Smith chart, as depicted in Fig. 17 by black triangular markers. Next, the action is repeated, while the adaptive loop is closed. For all hand positions the module input impedance now remains close to the center, as illustrated by the gray solid dots. For extreme hand-effects, the maximum module impedance correction is $-75j\Omega$. Hence, the module corrects antenna impedance disturbances as expected.

V. Conclusion

To improve link quality of cellular phones in fluctuating environments, we presented a multi-standard adaptively controlled series-LC matching network implemented with RF-MEMS capacitive switches.

Following a bottom-up approach, the design of an RF-MEMS unit cell for the construction of a 5-bit switched capacitor array has been described. Application-specific requirements on RF-MEMS have been derived, in particular on pull-in and pull-out voltage, resulting in the need for a high actuation voltage. For this purpose, a high-voltage driver IC has been developed that reduces dielectric charging of the MEMS devices by generating a bipolar waveform with small high/low duty-cycle to minimize the average actuation voltage.

We demonstrated proper correction of the reactance of a PIFA. For extreme hand-effects, the maximum module impedance correction at 900 MHz was $-75j\Omega$. The results prove the feasibility of RF-MEMS-based adaptive antenna matching modules, for application in multi-standard mobile phones.

Acknowledgment

The authors would like to acknowledge all their colleagues for contributions on RF-MEMS technology development, RF-MEMS modeling, characterization, packaging and reliability investigations. P. Lok and H. J. t. Dolle are acknowledged for their support to the AdAM project. Many thanks go to E. Cantatore for reviewing this manuscript. The authors are grateful to J. Sneep for designing the high-voltage driver IC and, last but not least, they owe much gratitude to K. Boyle for sharing his insights on antenna behavior.

References

[1] K. R. Boyle, "The performance of GSM 900 antenna in the presence of people and phantoms," in *IEEE Int. Conf. Antennas and Propagation*, Mar. 2003, vol. 1, pp. 35–38.

[2] G. F. Pedersen, K. Olesen, and S. L. Larsen, "Bodyloss for handheld phones," in *Proc. 49th IEEE Vehicular Technology Conf.*, May 1999, vol. 2, pp. 1580–1584.

[3] A. van Bezooijen, R. Mahmoudi, and A. H. M. van Roermund, "Adaptive methods to preserve power amplifier linearity under antenna mismatch conditions," *IEEE Trans. Circuits Syst. 1*, vol. 52, no. 10, pp. 2101–2108, Oct. 2005.

[4] A. Zolómy, R. Mernyei, J. Erdélyi, M. Pardoen, and G. Tóth, "Automatic antenna tuning for RF transmitter IC applying high Q antenna," in *Proc. IEEE RFIC Symp.*, Jun. 2004, pp. 501–504.

[5] O. Rostbakken, G. S. Hilton, and C. J. Railton, "An adaptive microstrip patch antenna for use in portable transceivers," in *Proc. IEEE Vehicular Technology Conf.*, May 1996, vol. 1, pp. 339–343.

[6] J. R. Moritz and Y. Sun, "Frequency agile antenna tuning and matching," in *Proc. IEE 8th Int. Conf. HF Radio Systems and Techniques*, Jul. 2000, pp. 169–174.

[7] M. Mileusnic, P. Petrociv, and J. Todorovic, "Design and implementation of fast antenna tuners for HF radiosystems," in *Proc. Int. Conf. Information, Communications and Signal Processing*, Sep. 1997, vol. 3, pp. 1722–1726.

[8] L.-Y. V. Chen, R. Forse, D. Chase, and R. A. York, "Analog tunable matching network using integrated thin-film BST capacitors," in *IEEE MTT-S Int. Microwave Symp. Dig.*, Jun. 2004, vol. 1, pp. 261–264.

[9] K. Buisman, "Distortion-free varactor diode topologies for RF adaptivity," in *IEEE MTT-S Int. Microwave Symp. Dig.*, Jun. 2005, pp. 157–160.

[10] D. Qiao, D. Choi, Y. Zhao, D. Kelly, T. Hung, D. Kimball, M. Li, and P. Asbeck, "Antenna impedance mismatch measurement and correction for adaptive CDMA tranceivers," in *IEEE MTT-S Int. Microwave Symp. Dig.*, Jun. 2005, pp. 783–786.

[11] A. Chamseddine, J. W. Haslett, and M. Okoniewski, "CMOS silicon-on-sapphire RF tunable matching networks," *EURASIP J. Wireless Commun. Netw.*, vol. 2006, pp. 1–11, 2006.

[12] J. Bonkowski and D. Kelly, "Integration of triple-band GSM antenna switch module using SOI CMOS," in *IEEE RFIC Symp. Dig.*, Jun. 2004, pp. 511–514.

[13] *RF MEMS Theory Design and Technology*, G. M. Rebeiz, Ed. New York: Wiley, 2003.

[14] *RF MEMS and Their Applications*, V. Varadan, K. J. Vinoy, and K. Jose, Eds. New York: Wiley, 2003.

[15] A. van Bezooijen, M. de Jongh, C. Chanlo, L. Ruijs, H. J. D. ten, P. Lok, F. van Straten, J. Sneep, R. Mahmoudi, and A. H. M. van Roermund, "RF-MEMS based adaptive antenna matching module," in *IEEE RFIC Symp. Dig.*, Jun. 2007, pp. 573–576.

[16] J. T. M. van Beek, "High-Q integrated RF passives and micro-mechanical capacitors on silicon," in *Proc. BCTM 2003*, Sep. 2003, pp. 147–150.

[17] A. J. M. de Graauw, P. G. Steeneken, C. Chanlo, S. Pramm, A. van Bezooijen, H. K. J. t. Dolle, F. van Straten, and P. Lok, "MEMS-based reconfigurable multi-band BiCMOS power amplifier," in *IEEE Proc. BCTM 2006*, Oct. 2006, pp. 17–20.

[18] F. Theunis, J. Bielen, M. de Jongh, and P. V. E. Krusemann, "A novel and efficient packaging technology for RF-MEMS devices," in *Proc. IEEE Electronic Components and Technology Conf.*, May 2007, pp. 1239–1245.

[19] F. Meng, A. van Bezooijen, and R. Mahmoudi, "A mismatch detector for adaptive impedance matching," in *Proc. 36th European Microwave Conf.*, Sep. 2006, pp. 1457–1460.

[20] *Analysis and Design of Analog Integrated Circuits*, P. R. Gray, P. J. Hurst, S. H. Lewis, and R. G. Meyer, Eds. New York: Wiley, 2001.

[21] K. R. Boyle, Y. Yuan, and L. P. Lighthart, "Analysis of mobile phone antenna impedance variations with user proximity," *IEEE Trans. Antennas Propagat.*, vol. 55, pp. 364–372, Feb. 2007.

[22] P. G. Steeneken, G. S. M. R. Th, J. T. M. van Beek, M. J. E. Ulenaers, J. de Coster, and R. Puers, "Dynamics and sqeeuze film gas damping of a capacitive RF MEMS switch," *J. Micromechan. Microeng.*, no. 15, pp. 176–184, Oct. 2004.

[23] V. Jiménez, J. Pons, M. Domínquez, A. Bermejo, L. Castaner, H. Nieminen, and V. Ermolov, "Transient dynamics of a MEMS variable capacitor driven with a Dickson charge pump," *Sensors and Actuators*, vol. A 128, pp. 89–97, 2006.

[24] T. Ranta, J. Ellä, and H. Pohjonen, "Antenna switch linearity requirements for GSM/WCDMA mobile phone front-ends," in *European Conf. Wireless Technology Dig.*, Oct. 2005, pp. 23–26.

[25] M. Innocent, P. Wambacq, S. Donnay, H. A. C. Tilmans, W. Sansen, and H. D. Man, "An analytic Volterra-series-based model for a MEMS variable capacitor," *IEEE Trans. Comput.-Aided Des. Integr. Circuits Syst.*, vol. 22, pp. 124–131, Feb. 2003.

André van Bezooijen (M'04) received the B.S. degree in electrical engineering from Breda Technical University, The Netherlands, in 1984. Currently, he is working towards the Ph.D. degree on adaptive RF front-ends.

Since 1998, he has been a Senior Engineer with Philips Semiconductors Nijmegen, The Netherlands, where, in the role of Project Leader, he was engaged in concept development of power amplifier and front-end modules for cellular phone applications. In 2006, the organization became part of NXP Semiconductors. He was involved in analog and mixed-signal integrated circuit design at Philips Research, Eindhoven, The Netherlands, from 1984 to 1993. From 1993 to 1998, he was with Philips Semiconductors System Laboratories, Eindhoven, where he worked on RF IC design and digital zero-IF receiver concepts. Since July 2008 he has been with EPCOS as RF System Architect, working on tunable RF front-ends. He is an author or coauthor of several papers and holds 12 patents.

Maurice A. de Jongh received the B.S. degree in electrical engineering from Eindhoven Polytechnic (Fontys) in 1999, and the M.Sc. degree (with honors) from Eindhoven University of Technology, Eindhoven, The Netherlands, in 2003.

From 1999 to 2003, he was with ECCT in Eindhoven, where he was working in the field of electromagnetic compatibility and compliance testing of phone equipment. In 2004, he joined Philips Semiconductors in Nijmegen, The Netherlands, as an RF Design Engineer, where he worked on matching circuits and filters in passive integration technology. In 2006, the organization became part of NXP semiconductors. Since March 2008 he has been with EPCOS. His interests are in the area of wireless communications, adaptive systems and RF-MEMS circuit concepts.

Christophe Chanlo received the M.Sc. degree in electrical engineering from the Northern Institute of Electronic and Microelectronic (University of Sciences and Technology of Lille), Lille, France.

After completion of his thesis at Philips Research, Eindhoven, The Netherlands, in 2000, he joined Philips Semiconductor in Nijmegen, The Netherlands, to work on integrated detectors for cellular phone applications. In 2006, the organization became part of NXP semiconductors. Since March 2008, he has been with EPCOS, involved in designing, modeling, and characterization of RF-MEMS-based adaptive modules.

Lennart C. H. Ruijs studied electrical engineering at Eindhoven University of Technology, Eindhoven, The Netherlands, where he joined the Mixed-signal Microelectronics Group in 2003. In April 2005, he received the M.Sc. degree with a thesis entitled "Breakdown Protection Circuits for Mobile Phone Power Amplifiers." For his graduation project, he worked together with Philips Semiconductors in Nijmegen, The Netherlands, where he continued his career. In 2006 the company became part of NXP Semiconductors, where he was working on analog and mixed-signal integrated circuits. Since March 2008 he has been with EPCOS, where he is involved in the design of RF-MEMS-based adaptive antenna matching systems.

Freek van Straten (M'00) studied electrical engineering and physics and received the M.Sc. degree from Eindhoven University of Technology, Eindhoven, The Netherlands.

He started working for Philips Semiconductors in Nijmegen, The Netherlands, in 1989 and since then has held positions as Development Manager for several RF system-in-package solutions. Since 2003, he has been a Senior Principal in the Business Unit Mobile and Personal working on architectures, technology, and products for cellular and connectivity standards. In 2006, the organization became part of NXP Semiconductors.

Reza Mahmoudi (M'99) studied electrical engineering at the Delft University of Technology, Delft, The Netherlands, where he joined the Microwave Component Group and received the M.Sc. degree in 1993 with a thesis entitled "A Measurement System for Noise Parameters." He was employed as a full member of the same group from January 1, 1993 to December 7, 1999. He earned the Designers Certificate from Delft in 1996 with a thesis entitled "A Systematic Design Method for a Feed-Forward Error Control System." This work was the initial step leading to his Ph.D. thesis.

He has worked for Philips Discrete Semiconductors in Nijmegen, The Netherlands, and Advanced Wave Research in El Segundo, CA. Since April 2003, he has been an Assistant Professor in the Department of Electrical Engineering at Eindhoven University of Technology.

Arthur H. M. van Roermund (SM'95) received the M.Sc. degree in electrical engineering from the Delft University of Technology, Delft, The Netherlands, in 1975, and the Ph.D. degree in Applied Sciences from the K.U.Leuven, Belgium, in 1987.

From 1975 to 1992, he was with Philips Research Laboratories in Eindhoven. From 1992 to 1999, he was a full Professor in the Electrical Engineering Department of Delft University of Technology, where he was Chairman of the Electronics Research Group and member of the management team of DIMES. From 1992 to 1999, he was Chairman of a two-years postgraduate school for "chartered designer." From 1992 to 1997, he was a consultant for Philips. In October 1999, he joined Eindhoven University of Technology as a full Professor, chairing the Mixed-Signal Microelectronics Group. Since September 2002, he has also been Director of Research of the Department of Electrical Engineering. He is Chairman of the Board of ProRISC, a nationwide microelectronics platform, and a member of the supervisory board of the NRC Photonics Research Centre. Since 2001, he has been one of the three organizers of the yearly workshop on Advanced Analog Circuit Design (AACD).

In 2004, Dr. van Roermund received the Simon Stevin Meester Award for his scientific and technological achievements.